New extrapolation method for low-lying states of nuclei in the *sd* and the *pf* shells

J. J. Shen,[1,2] Y. M. Zhao,[2,3,4,*] A. Arima,[2,5] and N. Yoshinaga[6]

[1]*Theoretical Nuclear Physics Laboratory, RIKEN Nishina Center, Wako 351-0198, Japan*

[2]*Department of Physics, Shanghai Jiao Tong University, Shanghai 200240, China*

[3]*Center of Theoretical Nuclear Physics, National Laboratory of Heavy Ion Accelerator, Lanzhou 730000, China*

[4]*CCAST, World Laboratory, P. O. Box 8730, Beijing 100080, China*

[5]*Musashi Gakuen, 1-26-1 Toyotamakami Nerima-ku, Tokyo 176-8533, Japan*

[6]*Department of Physics, Saitama University, Saitama 338-8570, Japan*

(Received 22 February 2011; published 27 April 2011)

We study extrapolation approaches to evaluate energies of low-lying states for nuclei in the *sd* and *pf* shells, by sorting the diagonal matrix elements of the nuclear shell-model Hamiltonian. We introduce an extrapolation method with perturbation and apply our new method to predict both low-lying state energies and $E2$ transition rates between low-lying states. Our predicted results arrive at an accuracy of the root-mean-squared deviations ∼40–60 keV for low-lying states of these nuclei.

DOI: 10.1103/PhysRevC.83.044322 PACS number(s): 21.10.Re, 23.20.Js, 24.10.Cn, 21.60.Cs

I. INTRODUCTION

The study of low-lying states is one of the most important topics in nuclear structure physics. Energy levels of low-lying states and electromagnetic transitions between these levels are among the fundamental properties of atomic nuclei. Theoretically, one of the most powerful approaches for studying the low-lying states is the nuclear shell model. The main problem, however, is that the shell-model space becomes gigantic when we study heavy nuclei. Diagonalization of the shell-model Hamiltonian becomes difficult. Therefore statistical methods and various truncations of the shell model are indispensable. There have been many attempts to evaluate the lowest eigenenergy for a given matrix of the nuclear shell-model Hamiltonian; see Refs. [1–13].

Recently, we suggested an extrapolation method to predict energies of the yrast states [14,15] by using a truncation based on sorting the diagonal matrix elements of the nuclear shell-model Hamiltonian. The procedure of this method is to diagonalize several sub-matrices of the full Hamiltonian whose dimension is less than 15% of the full space. In this paper, we present a more sophisticated study along the same lines. Here we study both energy levels and $E2$ transition rates for low-lying states.

In this paper the shell-model calculations are performed by using the shell-model code developed by the Kyushu group [16]. We take several sets of effective interactions, including the Yukawa [17], the USD [18], and the USDB [19] interactions for the *sd*-shell nuclei, and the Gaussian [17], the KB3 [20] and the GXPF1 [21] interactions for the *pf*-shell nuclei.

This paper is organized as follows. In Sec. II, we discuss our previous extrapolation method in evaluation of the lowest eigenvalue for spin-I states of the nuclear shell-model Hamiltonian. We make a comparison between our truncation scheme which is based on sorting the diagonal matrix elements of the shell-model Hamiltonian and a conventional truncation scheme based on sorting the single-particle energy term. In Sec. III we consider a perturbation in order to improve our previous method [14,15] and exemplify our new method by low-lying states of a few nuclei in the *sd* and the *pf* shells. We also extend our methods to evaluate electromagnetic quantities, such as $E2$ transition rates, electric quadrupole moments, and magnetic dipole moments of low-lying states for these nuclei. In Sec. IV we discuss the robustness of our new method with respect to the different sets of interactions and the size of the configuration space. In Sec. V we summarize the conclusions of this paper.

II. EXTRAPOLATION METHODS OF LOW-LYING STATE ENERGIES

We denote a matrix of the shell-model Hamiltonian H with dimension D and spin I by $H^{(I)}$ and its matrix elements by $H^{(I)}_{ij} = \langle\phi_i|H^{(I)}|\phi_j\rangle$, where ϕ_i and ϕ_j represent basis states with indices i and j, respectively. We sort the diagonal matrix elements $H^{(I)}_{ii}$ from the smaller to the larger. This sorting means nothing but a rearrangement for indices of basis states. We define the average magnitude of off-diagonal matrix elements by $M(t) = \sum_{i=1}^{D-t} |H^{(I)}_{i,i+t}|/(D-t)$, $t = 1, 2, 3, \ldots, D-1$, where t represents the "distance" from the diagonal matrix elements.

In Fig. 1, we show $M(t)$ for the $I^\pi = 2^+$ (π represents parity) states of ^{28}Si and ^{46}Ti, with and without sorting the diagonal elements $H^{(I)}_{ii}$ from the smaller to the larger. One sees that $M(t)$ with sorting $H^{(I)}_{ii}$ decreases gradually with t and becomes zero at $t = d_0$.

This feature provides us with a new clue to truncate the model space for the low-energy configurations. After sorting $H^{(I)}_{ii}$, we truncate the matrix $H^{(I)}$ artificially and obtain a series of Hamiltonian $h^{(I)}$ with dimension d ($d < D$), where $h^{(I)}_{ij} = H^{(I)}_{ij}$ ($i, j = 1, 2, \ldots, d$). This truncation scheme was

*Corresponding author: ymzhao@sjtu.edu.cn

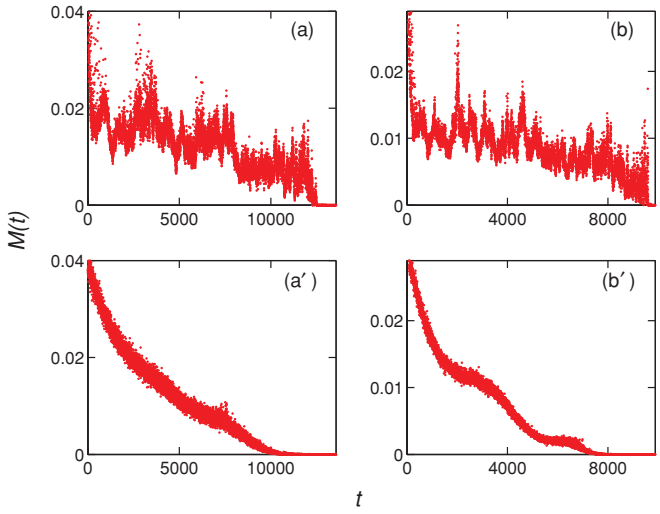

FIG. 1. (Color online) Average magnitudes [denoted by $M(t)$ in MeV] for off-diagonal matrix elements of $H^{(I)}$ with (the lower panels) and without (the upper panels) sorting the diagonal elements versus t, the "distance" with respect to the diagonal matrix elements. The panels on the left correspond to the $I^\pi = 2^+$ states of ^{28}Si by using the USDB interaction [19] and those on the right the $I^\pi = 2^+$ states of ^{46}Ti by using the GXPF1 interaction [21].

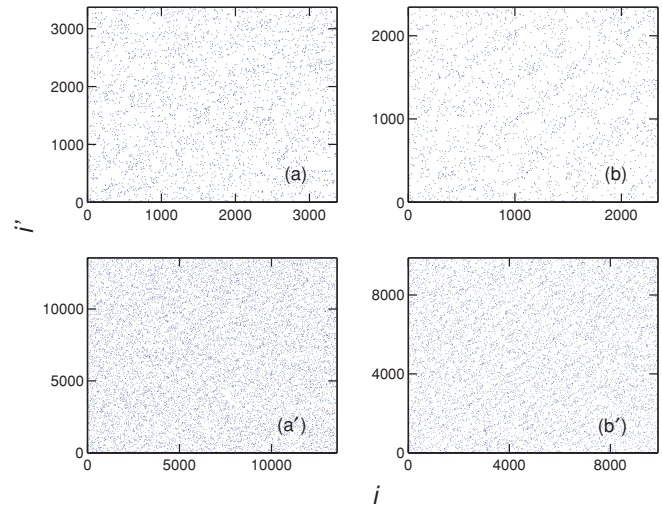

FIG. 2. (Color online) Correlation between the indices of basis states sorted by single-particle configurations and the diagonal elements of $H^{(I)}$. Each datum corresponds to one set of $[H'_{ii}(I), H''_{i'i'}(I)]$, with $H'_{ii}(I) = H''_{i'i'}(I)$. We take the USDB [19] interaction for ^{28}Si and the GXPF1 interaction [21] for ^{46}Ti. (a) $I = 0$ states for ^{28}Si; (b) $I = 0$ states for ^{46}Ti; (a′) $I = 2$ states for ^{28}Si; (b′) $I = 2$ states for ^{46}Ti. See the text for details.

used to evaluate the lowest eigenvalue of spin-I states in Refs. [14,15].

A conventional truncation scheme of the shell-model space is based on sorting the single-particle energies. Because the magnitudes of the single-particle energy term of $H^{(I)}$ are much larger than those of two-body interactions, configurations which have smaller values of single-particle energies are usually assumed to play the dominant role in low-lying states, whereas those have larger values of single-particle energies are assumed to be less important. However, there are also considerably large contributions in $H^{(I)}$ from the two-body interactions. Let us denote the matrix of $H^{(I)}$ with sorting the diagonal matrix elements by $H'(I)$ and the matrix of $H^{(I)}$ with sorting the single-particle energy term by $H''(I)$. The diagonal matrix element $H'_{ii}(I)$ locates at the i-th row and the i-th column for $H'(I)$, but it moves to the i'-th row and the i'-th column in $H''(I)$. If i and i' are always the same or very close, these two truncations are equivalent or very close to each other. However, this is not the case for realistic nuclei; instead, i and i' differ from each other substantially. In Fig. 2, we investigate whether there are any correlations between i and i' for ^{28}Si and ^{46}Ti. No correlation is noted between them.

One thus asks the following question: Which truncation scheme is more efficient, the one based on sorting the diagonal matrix elements or the one based on sorting the single-particle energy term? In Fig. 3, we present the overlaps between the wave functions calculated by the exact diagonalizations of $H^{(I)}$ and those by truncating the matrix $H^{(I)}$ to $h^{(I)}$, in terms of $\ln(D/d)$. $h^{(I)}_{ij} = H^{(I)}_{ij}$ for $i, j \leqslant d$, with $H^{(I)}_{ij}$ rearranged by sorting either the diagonal matrix elements or the single-particle energy term. One sees that the truncation by sorting the diagonal matrix elements $H^{(I)}_{ii}$ is more efficient: The overlaps for truncations by sorting $H^{(I)}_{ii}$ (results in red in Fig. 3) are systematically larger than overlaps for truncations by sorting the single-particle energy term (results in blue in Fig. 3). Furthermore, the overlaps for truncations based on sorting $H^{(I)}_{ii}$ change gradually with $\ln(d)$, instead of sudden changes. This property is important for extrapolations.

After diagonalizing $h^{(I)}$, we obtain its lowest eigenenergy, ε_d. According to Refs. [14,15], ε_d is linear in terms of $\ln(d)$ when d is less than d_0, and changes its slope at $d = d_0$ (d_0 was determined by $M(d_0) = 0$ in Ref. [14]; in this paper we assume empirically $d_0 = 0.75D$). The predicted lowest energy of spin-I states is given by

$$E^{(I)}_{\min} = 0.4\ln D + 0.6k\ln d_0 + b, \tag{1}$$

where k and b are the slope and the intercept of the ε_d-ln$d$ plot for $d < d_0$, respectively. The values of k and b can be obtained by a few matrices $h^{(I)}$ with $d \ll D$ [14].

We denote the second (third) lowest spin-I state energy by using $E^{(I)}_{(1)}$ ($E^{(I)}_{(2)}$), and the second (third) lowest eigenvalue of $h^{(I)}$ by $\varepsilon^{(1)}_d$ ($\varepsilon^{(2)}_d$). In Fig. 4, we present correlations of ε_d, $\varepsilon^{(1)}_d$, and $\varepsilon^{(2)}_d$ versus $\ln(D/d)$, where it is seen that these correlations are very similar to each other. Similar to Eq. (1), we empirically assume that

$$E^{(I)}_{(1)} = 0.4\ln D + 0.6k_1\ln d_0 + b_1, \tag{2}$$

$$E^{(I)}_{(2)} = 0.4\ln D + 0.6k_2\ln d_0 + b_2, \tag{3}$$

where k_1, k_2 and b_1, b_2 are the slopes and intercepts in the $\varepsilon^{(1)}_d$-ln$d$ and $\varepsilon^{(2)}_d$-ln$d$ plots for $d < d_0$. These parameters can be calculated by in the same way as for k and b in Eq. (1).

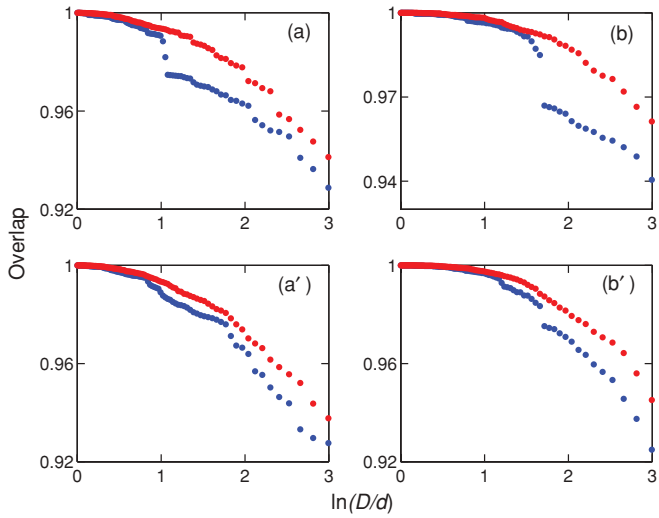

FIG. 3. (Color online) Overlaps between wave functions calculated by exact diagonalizations of $H^{(I)}$ and those by diagonalizing truncated matrices $h^{(I)}$ versus $\ln(D/d)$. $h^{(I)}_{ij} = H^{(I)}_{ij}$ for $i, j \leqslant d$. The results in red (blue) correspond to truncations by sorting $H^{(I)}_{ii}$ (single-particle energies). One sees that the overlaps for truncations based on sorting $H^{(I)}_{ii}$ increase gradually with $\ln(d)$ and are systematically larger than those for truncations based on sorting single-particle energies. (a) $I = 0$ states for ^{28}Si; (b) $I = 0$ states for ^{46}Ti; (a′) $I = 2$ states for ^{28}Si; (b′) $I = 2$ states for ^{46}Ti.

III. EXTRAPOLATION METHOD WITH PERTURBATION

In this section we improve our extrapolation method by applying the perturbation theory of stationary states in quantum mechanics. We rewrite the Hamiltonian $H^{(I)} = H^{(I)}_0 + (H^{(I)} - H^{(I)}_0) = H^{(I)}_0 + H'^{(I)}$, where $(H^{(I)}_0)_{ij} = h^{(I)}_{ij}$ for $i, j \leqslant d$ and $(H^{(I)}_0)_{ij} = \delta_{ij} H^{(I)}_{ii}$ for i or $j > d$. Here the matrix $H^{(I)}$ is given with sorting diagonal matrix elements from the smaller to the larger, and $H^{(I)}_{ij} = \langle \phi_i | H^{(I)} | \phi_j \rangle$. Namely

$$H^{(I)}_0 = \begin{pmatrix} h^{(I)} & 0 & 0 & \dots & 0 \\ 0 & H^{(I)}_{d+1,d+1} & 0 & \ddots & 0 \\ 0 & 0 & H^{(I)}_{d+2,d+2} & \ddots & \vdots \\ \vdots & \vdots & \ddots & \ddots & \vdots \\ 0 & 0 & 0 & \dots & H^{(I)}_{D,D} \end{pmatrix},$$

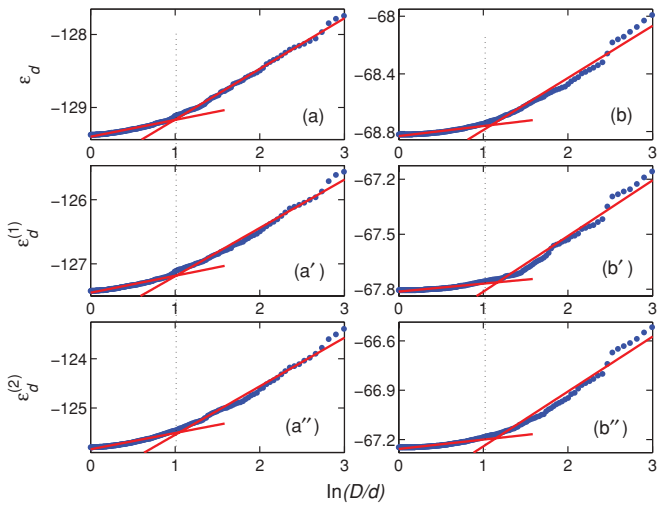

FIG. 4. (Color online) Energies (in MeV) of the three lowest states [denoted by ε_d, $\varepsilon^{(1)}_d$, and $\varepsilon^{(2)}_d$] of $h^{(I)}$ versus $\ln(D/d)$. The three panels on the left (right) correspond to ^{28}Si (^{46}Ti). One sees that correlations in the ε_d-$\ln(D/d)$, $\varepsilon^{(1)}_d$-$\ln(D/d)$ and $\varepsilon^{(2)}_d$-$\ln(D/d)$ plots are very similar. The vertical dashed lines are plotted to highlight d_0. The solid straight lines in red are optimized to fit ε_d, $\varepsilon^{(1)}_d$, and $\varepsilon^{(2)}_d$ for both $d \geqslant d_0$ and $d \leqslant d_0$.

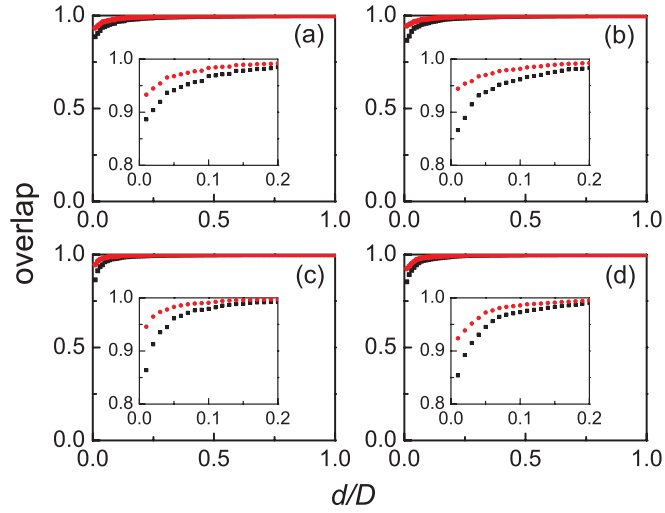

FIG. 5. (Color online) Overlaps $|\langle \Psi^P(d) \mid \Phi \rangle|$ (in red) and $|\langle \Psi(d) \mid \Phi \rangle|$ (in black) d/D. The panels on the left (right) correspond to ^{28}Si (^{46}Ti). $I = 0$ in the upper panels, and $I = 2$ in the lower ones.

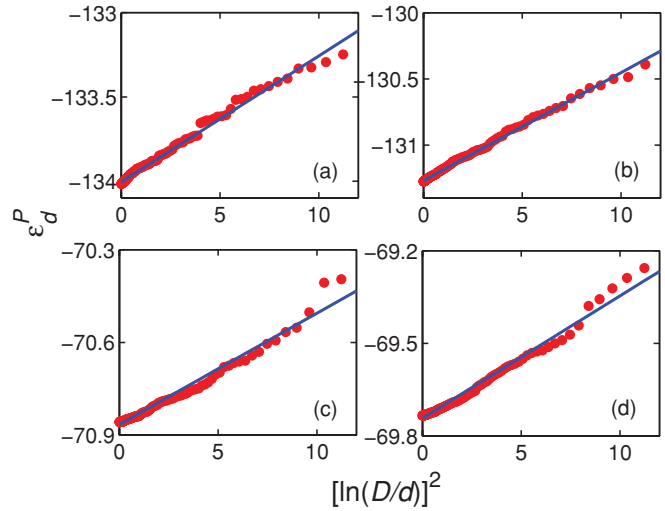

FIG. 6. (Color online) The lowest energy (in MeV) of $H^{(I)}_0$ with perturbation (denoted by ε^P_d) versus $[\ln(D/d)]^2$. The panels on the left (right) correspond to ^{28}Si (^{46}Ti). $I = 0$ in the upper panels, and $I = 2$ in the lower ones.

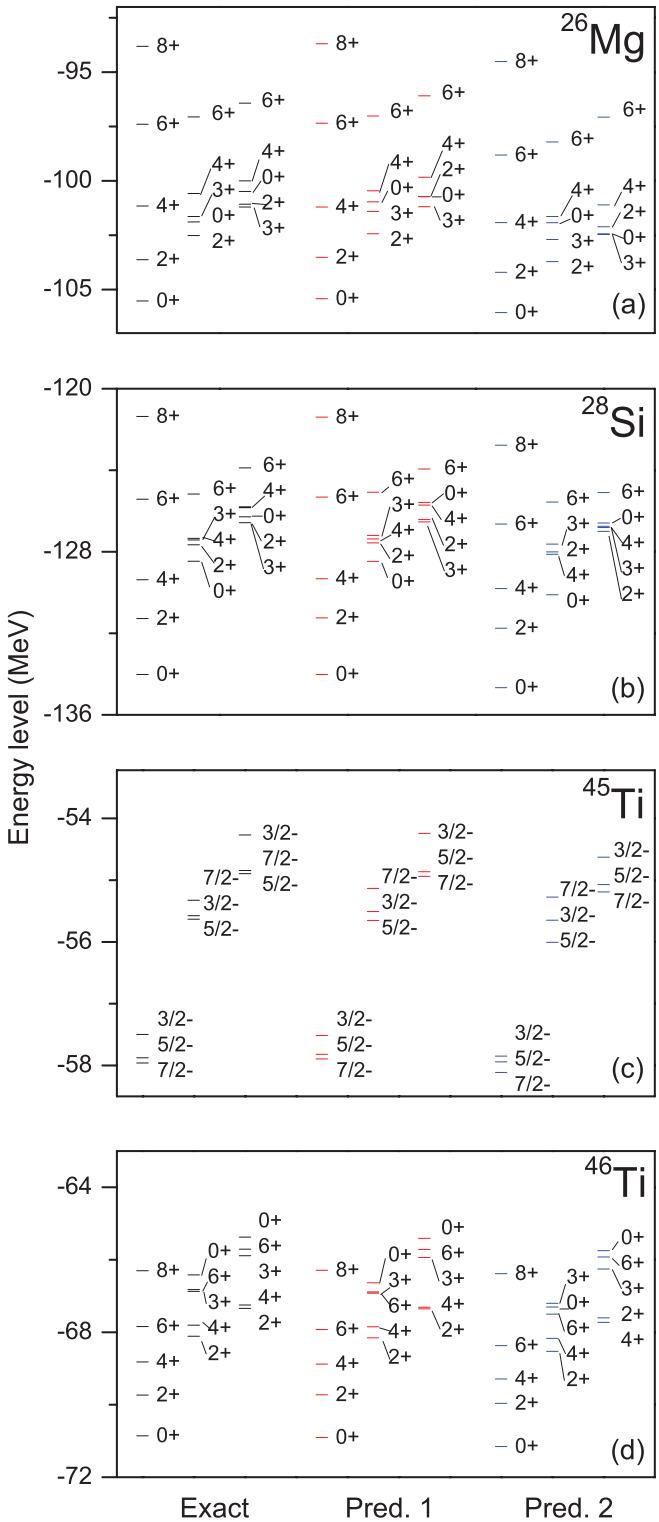

FIG. 7. (Color online) Energy levels (energies in MeV) based on the diagonalizations of $H^{(I)}$ (denoted by "Exact"), the extrapolation with perturbation (denoted by "Pred.1"), and the extrapolation without perturbation (denoted by "Pred.2"). In these predictions, we use up to 15% of the full space for each $H^{(I)}$, i.e., $d/D \leqslant 0.15$. (a) ^{26}Mg, (b) ^{28}Si, (c) ^{45}Ti, and (d) ^{46}Ti. We take the USDB interaction in (a) and (b), and the GXPF1 interaction in (c) and (d).

TABLE I. Root-mean-squared deviations (RMSD) of predicted yrast-state energies of ^{26}Mg, ^{28}Si, and ^{45,46}Ti. δ_1 and δ_2 correspond to the RMSD by using Eqs. (6) and (1), respectively. One see that δ_1 is approximately 10 times smaller than δ_2.

Nuclei	δ_1 (keV)	δ_2 (keV)
^{26}Mg	89.9	868.9
^{28}Si	56.6	914.7
^{45}Ti	50.8	415.5
^{46}Ti	49.8	565.5

$H_0^{(I)}$ is the dominant "unperturbed" part of $H^{(I)}$, and $H'^{(I)}$ is the small "perturbation" part. To proceed, we diagonalize $H_0^{(I)}$. This is essentially the diagonalization of $h^{(I)}$ (for $d \ll D$), as in Refs. [14,15]. We denote the lowest-energy wave function of $H^{(I)}$ by Φ, the lowest-energy wave function of $h^{(I)}$ by $\Psi(d)$, and the lowest-energy wave function of $H_0^{(I)}$ with the first-order perturbation by $\Psi^P(d)$,

$$\Psi^P(d) = \Psi(d) + \sum_{i=d+1}^{D} \phi_i \frac{\sum_{j=1}^{d} \Psi_j(d) H'^{(I)}_{ji}}{\varepsilon_d - H^{(I)}_{ii}}, \tag{4}$$

where $\Psi_j(d)$ is the j-th component of $\Psi(d) = \sum_{j=1}^{d} \Psi_j \phi_j$, ε_d is the lowest energy of $h^{(I)}$, $H'^{(I)}_{ji} \equiv H^{(I)}_{ji}$, and $H^{(I)}_{ii} = H^{(I)}_{0,ii}$ $\Psi^P(d)$ is not normalized in Eq. (4).

In Fig. 5, $\langle \Psi^P(d) | \Phi \rangle$ and $\langle \Psi(d) | \Phi \rangle$ versus d/D are presented for the lowest $I^\pi = 0^+$ and $I^\pi = 2^+$ states of two nuclei, ^{28}Si and ^{46}Ti. One sees that $\langle \Psi^P(d) \mid \Phi \rangle$ and $\langle \Psi(d) \mid \Phi \rangle$ increase quickly with d/D and saturate to 1.0 at $d/D \sim 0.05 - 0.10$ and that the perturbation improves the wave functions when $d < 0.1D$ [i.e., $\Psi^P(d)$ has a larger overlap with Φ than $\Psi(d)$].

By using the above $\Psi^P(d)$, we predict the lowest eigenenergy (denoted by ε_d^P) of $H_0^{(I)}$ with the second-order perturbation

$$\varepsilon_d^P = \varepsilon_d + \sum_{i=d+1}^{D} \frac{\left(\sum_{j=1}^{d} \Psi_j(d) H'^{(I)}_{ji}\right)^2}{\varepsilon_d - H^{(I)}_{ii}}, \tag{5}$$

where ε_d is the lowest energy of $h^{(I)}$ and d is the dimension of $h^{(I)}$. The first-order correction is zero for ε_d^P, because $H'^{(I)}_{ii} \equiv 0$.

In Fig. 6, we show a few correlations between ε_d^P and $[\ln(D/d)]^2$, for the $I^\pi = 0^+$ and $I^\pi = 2^+$ states of ^{28}Si by using the USDB interaction and ^{46}Ti by using the GXPF1 interaction. One notices an approximate linear correlation between ε_d^P and $[\ln(D/d)]^2$. Based on this empirical correlation, we assume that

$$\varepsilon_d^P = E^{(I)}_{\min} + a[\ln(D/d)]^2, \tag{6}$$

where $E^{(I)}_{\min}$ is the lowest eigenvalue of spin-I states. The parameter a is obtained by optimizing the linear correlation between ε_d^P and $[\ln(D/d)]^2$ for a few $h^{(I)}$ with $d \ll D$. Thus we obtain $E^{(I)}_{\min}$ by diagonalizing a few $h^{(I)}$. Without details we note that the evaluations of nonyrast state energies are the same as Eq. (6) except that the value of parameter a is different.

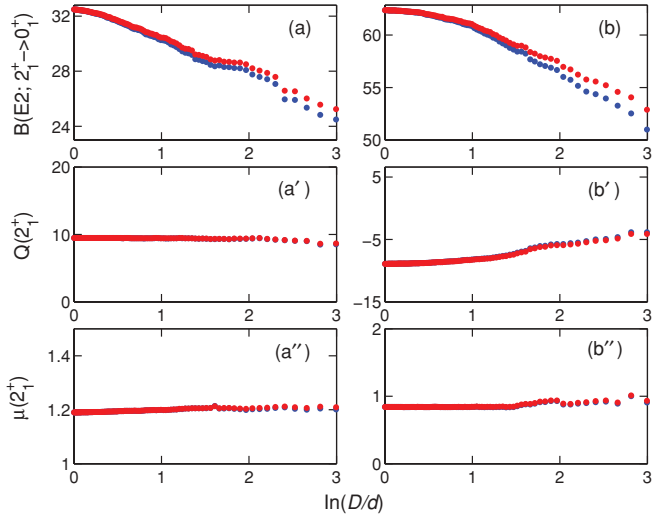

FIG. 8. (Color online) $B(\mathrm{E2}, 2^+ \to 0^+)$ (in e^2 fm^4), electric quadrupole moments Q (in e fm^2), and magnetic dipole moments μ (in μ_N) versus $\ln(D/d)$. The panels on the left correspond to ^{28}Si by using the USDB interaction [19] and those on the right ^{46}Ti by using the GXPF1 interaction [21].

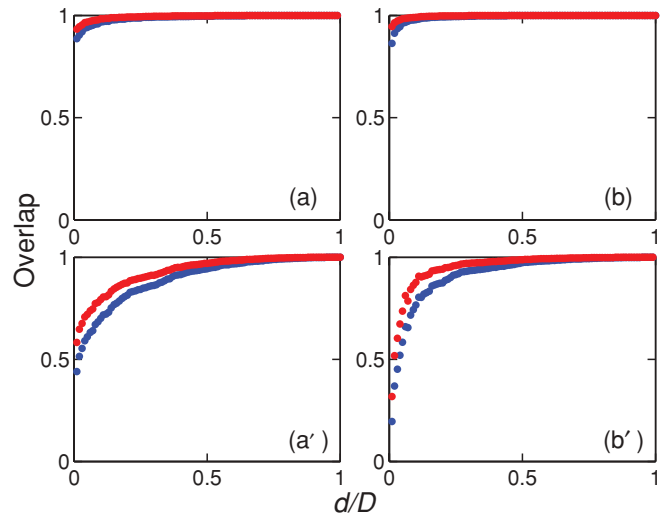

FIG. 9. (Color online) Overlaps $|\langle\Psi^P(d) \mid \Phi\rangle|$ (in red) and $|\langle\Psi(d) \mid \Phi\rangle|$ (in blue) for the 0_1^+ state of ^{28}Si (panels on the left) and ^{46}Ti (panels on the right) versus d/D. We show the USDB, the GXFP1, the Yukawa, and the Gaussian interactions in panels (a), (b), (a′), and (b′), respectively.

In Fig. 7 we present low-lying states predicted by using two extrapolation methods: extrapolation with perturbation, denoted by "Pred.1," and extrapolation without perturbation, denoted by "Pred. 2," for ^{26}Mg, ^{28}Si, ^{46}Ti, and ^{45}Ti. In our predictions, we use the 15% of the full space for each $H^{(I)}$. The predicted energy levels are compared with those calculated by the exact diagonalizations of $H^{(I)}$. One see in Fig. 7 that both methods approximately reproduce low-lying states calculated by exact diagonalizations. In Table I, we show the root-mean-squared deviations (RMSD) of these two methods. One sees that the extrapolation method with perturbation (i.e., "Pred.1") is superior to extrapolation without perturbation (i.e., "Pred.2"): The RMSD's from the former method are smaller than those by using the latter method by a factor of about 10.

In Fig. 5, we have shown that the overlap $|\langle\Psi^P(d) \mid \Phi\rangle|$ increases with d and saturates to 1.0 when $d/D \geqslant 0.10$. Thus we expect our extrapolation method be useful in predicting electromagnetic quantities. In Fig. 8, we present $E2$ transition rates, quadrupole moments, and magnetic moments in terms of $\ln(D/d)$ for ^{24}Mg, ^{28}Si, ^{45}Ti, and ^{46}Ti, where we take two set of wave functions: (i) the lowest-energy wave function of $H_0^{(I)}$ with the first-order perturbation, i.e., $\Psi^P(d)$ in Eq. (4), and (ii) the lowest-energy wave function of $h^{(I)}$, i.e., $\Psi(d)$. In Table II, we tabulate our predicted results by using these two sets of wave functions, in comparison with those calculated by exact diagonalizations of $H^{(I)}$. Both of them are found to work reasonably well, with the one by using $\Psi^P(d)$ [wave function of $h^{(I)}$ with perturbation] slightly more efficient. Here we use up to the 15% of the full model space (i.e., $d/D \leqslant 0.15$) in predicting these results, as in Fig. 7.

TABLE II. Predicted $E2$ transition rates (in e^2 fm^4), electric quadrupole moments Q (in e fm^2), and magnetic dipole moments μ (in μ_N) in comparison with those calculated by the exact diagonalizations (denoted by "Exact"). "Pred.1" and "Pred.2" are based on $\Psi^P(d)$ and $\Psi(d)$, respectively.

$B(E2)$	I^π	Exact	Pred.1	Pred.2
^{24}Mg	$2_1^+ \to 0_1^+$	76.85	65.49	70.94
^{28}Si	$2_1^+ \to 0_1^+$	32.40	31.61	35.82
^{45}Ti	$3/2_1^- \to 7/2_1^-$	54.53	53.70	66.82
^{46}Ti	$2_1^+ \to 0_1^+$	62.36	61.01	66.10
Q	I^π	Exact	Pred.1	Pred.2
^{24}Mg	2_1^+	−17.46	−17.16	−18.41
^{28}Si	2_1^+	9.46	9.90	10.51
^{45}Ti	$7/2_1^-$	−5.58	−5.46	−6.37
^{46}Ti	2_1^+	−8.90	−7.25	−8.84
μ	I^π	Exact	Pred.1	Pred.2
^{24}Mg	2_1^+	1.03	1.06	1.07
^{28}Si	2_1^+	1.19	1.19	1.18
^{45}Ti	$7/2_1^-$	−0.15	−0.04	−0.07
^{46}Ti	2_1^+	0.84	0.90	0.91

TABLE III. The RMSD (in keV) of predicted energies by using our new extrapolation method. We use the USDB and Yukawa interactions for ^{28}Si and the GXPF1 and Gaussian interactions for ^{46}Ti.

I^π	^{28}Si		^{46}Ti	
	USDB	Yukawa	GXPF1	Gaussian
0_1^+	3.9	926.7	48.6	400.1
2_1^+	34.7	1119.1	9.4	1103.8
4_1^+	52.0	637.1	59.3	1385.8

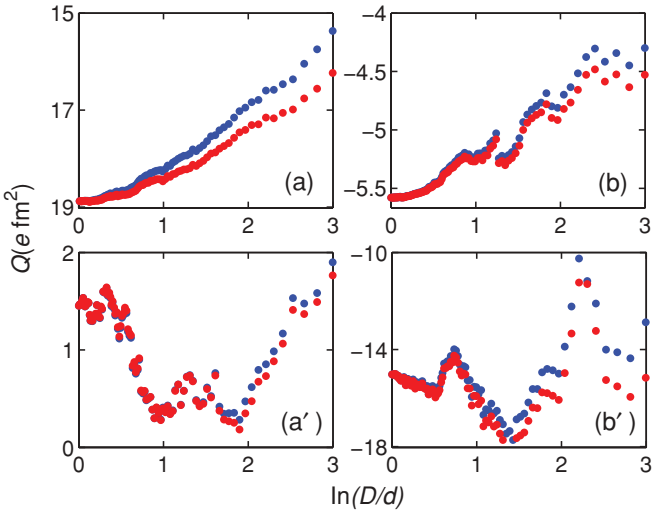

FIG. 10. (Color online) Quadrupole moments Q (in e fm^2) versus $\ln(D/d)$. The results in red (blue) are obtained by using extrapolation with (without) perturbation. The panels on the left correspond to the first $I^\pi = (5/2)^+$ state of ^{25}Mg and those on the right correspond to the first $I^\pi = (7/2)^-$ state of ^{45}Ti. We use the USDB, the GXPF1, the Yukawa, and the Gaussian interactions in (a), (b), (a′), and (b′), respectively.

IV. ROBUSTNESS OF OUR EXTRAPOLATION METHOD

In Sec. III we have shown that our new extrapolation method is very efficient in predicting both low-lying state energies and $E2$ transition rates for nuclei in the sd shell and in the pf shell by using realistic effective interactions. One would ask whether this new method is robust if we use an interaction which is not well refined and whether this method continues to work well for matrices with larger dimensions.

In Fig. 9, we present $|\langle\Psi^P(d)|\Phi\rangle|$ and $|\langle\Psi(d)|\Phi\rangle|$ for the $I^\pi = 0_1^+$ states of ^{28}Si and ^{46}Ti. In the upper two panels we use interactions which are well refined, the USDB interaction for ^{28}Si in (a) and the GXPF1 interaction for ^{46}Ti in (b), and in the lower panels we use the interactions which are not well refined, the Yukawa interaction for ^{28}Si in (a′) and the Gaussian interaction for ^{46}Ti in (b′). One easily notices that the values of overlaps in the upper panels saturate to 1.0 at a much smaller value of d/D than those in the lower panels, in which we use the Yukawa or Gaussian interaction.

In Table III, we present the RMSD of our predicted energies by using Eq. (6), with $d/D \leqslant 0.15$. For ^{28}Si we use the USDB and Yukawa interactions, and for ^{46}Ti we use the GXPF1 and Gaussian interactions. One sees that the RMSD by using the refined realistic interactions are one or two orders smaller than

TABLE IV. The RMSD's by using Eq. (6) for ^{26}Mg, ^{26}Mg, ^{28}Si, ^{26}Al, ^{27}Si, ^{46}Ti, ^{26}Al, and ^{45}Ti. Here we use the GXPF1 interaction for ^{45,46}Ti and the USDB interaction for others.

Nucleus	^{24}Mg	^{25}Mg	^{26}Mg	^{26}Al
RMSD	823.2	288.8	89.9	422.8
Nucleus	^{27}Si	^{28}Si	^{45}Ti	^{46}Ti
RMSD	201.8	56.6	50.8	49.8

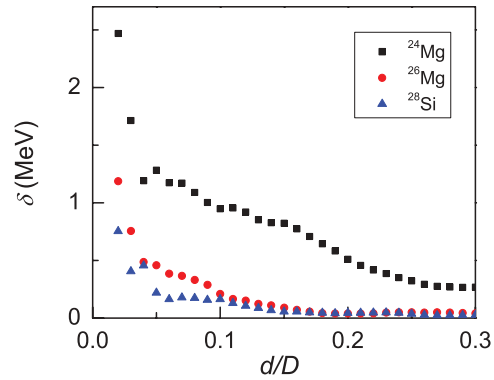

FIG. 11. (Color online) The RMSD (in MeV) of predicted energies by using Eq. (6) versus d/D, for ^{24}Mg (dimension D from 900 to 5000), ^{26}Mg (dimension D from 1900 to 9000), and ^{28}Si (dimension from 3000 to 16 000). One sees that the RMSD is smaller for systems with larger D. Here we use the USDB interaction.

those by using interactions which are not well refined (here the Yukawa and Gaussian interactions).

In Fig. 10 we present electric quadrupole moments in terms of $\ln(D/d)$ for the yrast $I^\pi = (5/2)^+$ state of ^{25}Mg by using the USDB and the Yukawa interactions, and for

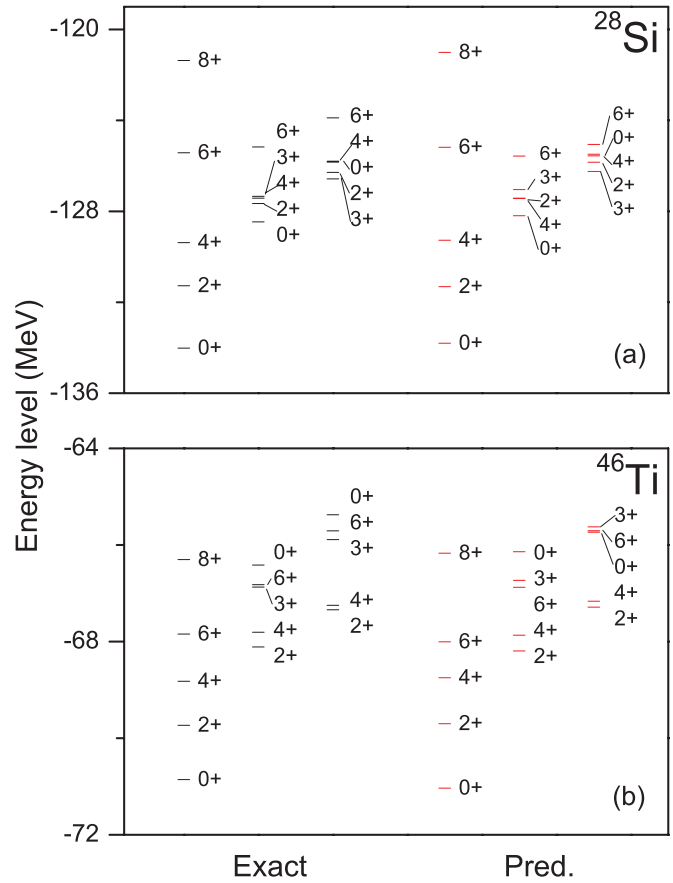

FIG. 12. (Color online) Predicted energy levels by using our new extrapolation method in comparison with those by exact diagonalizations. (a) ^{28}Si by using the USDB interaction; (b) ^{46}Ti by using the GXPF1 interaction. See the text for details.

the yrast $I^\pi = 7/2^-$ state of ^{45}Ti by using the GXPF1 and Gaussian interactions, with and without perturbation. One sees that the extrapolations do not work well if we use the Yukawa interaction or the Gaussian interaction (see the lower panels in Fig. 10). These numerical experiments show that the extrapolations become irregular and less efficient if the interaction deviates largely from the "realistic" interaction. Thus our extrapolation may be useful as a touchstone of the interactions in parametrizations.

Now we investigate the robustness of our extrapolation method with respect to D, the dimension of $H^{(I)}$. In Table IV, we tabulate the RMSD's given by our extrapolation method for ^{24}Mg, ^{25}Mg, ^{26}Mg, ^{26}Al, ^{27}Si, and ^{28}Si by using the USDB interaction, ^{45}Ti and ^{46}Ti by using the GXPF1 interaction. According to Table IV, the RMSD values decrease with D. This suggests that our extrapolation method with perturbation is more efficient for matrices with larger dimensions. In other words, one needs a smaller portion for a matrix with larger dimensions in order to achieve a reasonable accuracy of evaluated eigenvalues by using our extrapolation method.

We exemplify the feature exhibited in Table IV by using ^{24,26}Mg and ^{28}Si. We apply our new extrapolation method to predict the low-lying levels of these nuclei and calculate the RMSD for d/D ranging from 0.02 to 0.3. We present our calculated RMSD in Fig. 11. One sees that these RMSD values are smaller for nuclei with larger D and that they decrease rapidly with d/D.

In Fig. 12 we present our predicted low-lying states by using our new extrapolation method. We use up to 5% of the total space (i.e., $d/D \leqslant 0.05$) for ^{28}Si and 3% for ^{46}Ti. The RMSD is 189.7 keV for ^{28}Si and 115.0 keV for ^{46}Ti.

V. SUMMARY

To summarize, in this paper we study extrapolation methods in studying low-lying states of a few nuclei in the sd and the pf shells by sorting the diagonal matrix elements $H^{(I)}_{ii}$ of the nuclear shell-model Hamiltonian matrix $H^{(I)}$.

First, we discuss our extrapolation method of Refs. [14,15]. We make comparisons between our present truncation scheme which is based on sorting the diagonal matrix elements of $H^{(I)}$ and the conventional truncation scheme which is based on sorting single-particle configurations. We conclude that sorting the diagonal elements of $H^{(I)}$ provides us with a new and more efficient truncation scheme of the full shell-model space.

Second, we apply the perturbation theory to improve our previous extrapolation method and exemplify our new method by using low-lying states of a few nuclei in the sd shell and in the pf shell. Our predicted results based on diagonalizing a few submatrices of $H^{(I)}$ with $d/D \leqslant 15\%$ [d is the dimension of truncated matrix $h^{(I)}$ and D is that of the matrix $H^{(I)}$] arrive at an accuracy of the RMSD ~ 50 keV for low-lying states of nuclei in the sd and pf shells. These RMSD values are about 10 times smaller than our previous method [14,15]. We also extend our new extrapolation method to predict $E2$ transition rates, electric quadrupole moments, and magnetic moments. Our predicted results of these quantities are also in good agreement with exact solutions.

Third, we notice two features exhibited in our new extrapolation method: (i) This method works well if we use "good" effective interactions. If we use an interaction which is not well refined (e.g., the Yukawa interaction), it becomes less efficient. (ii) According to our numerical experiments so far, the new method is more efficient when one goes to matrices with larger dimensions. These two features are potentially very important, because they suggests that our new method might be useful in evaluating the effective interactions as touchstone and also in studying the nuclear structure of nuclei not accessible by exact diagonalizations of $H^{(I)}$ due to the large dimensionality of configuration spaces.

ACKNOWLEDGMENT

We thank the National Natural Science Foundation of China for supporting this work under Grant No. 10975096 and the Chinese Major State Basic Research Developing Program under Grant No. 2007CB815000.

[1] K. F. Ratcliff, Phys. Rev. C **3**, 117 (1971).
[2] F. J. Margetan, A. Klar, and J. P. Vary, Phys. Rev. C **27**, 852 (1983).
[3] V. Velázquez and A. P. Zuker, Phys. Rev. Lett. **88**, 072502 (2002).
[4] T. Papenbrock and H. A. Weidenmuller, Phys. Rev. Lett. **93**, 132503 (2004); Phys. Rev. C **73**, 014311 (2006).
[5] T. Papenbrock and H. A. Weidenmueller, Rev. Mod. Phys. **79**, 997 (2007); H. A. Weidenmueller and G. E. Mitchell, Rev. Mod. Phys. **81**, 539 (2009).
[6] N. Yoshinaga, A. Arima, and Y. M. Zhao, Phys. Rev. C **73**, 017303 (2006).
[7] J. J. Shen, Y. M. Zhao, A. Arima, and N. Yoshinaga, Phys. Rev. C **77**, 054312 (2008).
[8] J. J. Shen, A. Arima, Y. M. Zhao, and N. Yoshinaga, Phys. Rev. C **78**, 044305 (2008); N. Yoshinaga, A. Arima, J. J. Shen, and Y. M. Zhao, *ibid.* **79**, 017301 (2009).
[9] L. H. Zhang, J. J. Shen, Y. Lei, and Y. M. Zhao, Int. J. Mod. Phys. E **17**, 342 (2008).
[10] S. E. Koonin, D. J. Dean, and K. Langanke, Phys. Rep. **577**, 1 (1996); T. Otsuka, M. Honma, T. Mizusaki, N. Shimizu, and Y. Utsuno, Prog. Part. Nucl. Phys. **47**, 319 (2001).
[11] M. Horoi, A. Volya, and V. Zelevinsky, Phys. Rev. Lett. **82**, 2064 (1999); M. Horoi, J. Kaiser, and V. Zelevinsky, Phys. Rev. C **67**, 054309 (2003).
[12] T. Mizusaki and M. Imada, Phys. Rev. C **67**, 041301 (2003); T. Mizusaki, *ibid.* **70**, 044316 (2004).
[13] T. Papenbrock, A. Juodagalvis, and D. J. Dean, Phys. Rev. C **69**, 024312 (2004); W. G. Wang, Phys. Rev. E **63**, 036215 (2001).
[14] J. J. Shen, Y. M. Zhao, and A. Arima, Phys. Rev. C **82**, 014309 (2010).
[15] N. Yoshinaga and A. Arima, Phys. Rev. C **81**, 044316 (2010).
[16] K. Takada [http://ftp.kutl.kyushu-u.ac.jp/pub/takada/jjSMQ/].

[17] T. Inoue, T. Sebe, H. Hasegawa, and A. Arima, Nucl. Phys. **59**, 1 (1964); Y. Akiyama, A. Arima, and T. Sebe, Nucl. Phys. A **138**, 273 (1969).
[18] B. H. Wildenthal, Prog. Part. Nucl. Phys. **11**, 5 (1984); B. A. Brown and B. H. Wildenthal, Annu. Rev. Nucl. Part. Sci. **38**, 29 (1988).
[19] B. A. Brown and W. A. Richter, Phys. Rev. C **74**, 034315 (2006).
[20] A. Poves and A. P. Zuker, Phys. Rep. **70**, 235 (1981).
[21] M. Honma, T. Otsuka, B. A. Brown, and T. Mizusaki, Phys. Rev. C **69**, 034335 (2004).